Mode characteristics of metallically coated square microcavity connected with an output waveguide

Kai-Jun Che and Yong-Zhen Huang[a)]
State Key Laboratory on Integrated Optoelectronics, Institute of Semiconductors, Chinese Academy of Sciences, P.O. Box 912, Beijing 100083, People's Republic of China

(Received 4 January 2010; accepted 23 April 2010; published online 2 June 2010)

Mode characteristics of a square microcavity with an output waveguide on the middle of one side, laterally confined by an insulating layer SiO_2 and a *p*-electrode metal Au, are investigated by two-dimensional finite-difference time-domain technique. The mode quality (Q) factors versus the width of the output waveguide are calculated for Fabry–Pérot type and whispering-gallery type modes in the square cavity. Mode coupling between the confined modes in the square cavity and the guided modes in the output waveguide determines the mode Q factors, which is greatly influenced by the symmetry behaviors of the modes. Fabry–Pérot type modes can also have high Q factors due to the high reflectivity of the Au layer for the vertical incident mode light rays. For the square cavity with side length 4 μm and refractive index 3.2, the mode Q factors of the Fabry–Pérot type modes can reach 10^4 at the mode wavelength of 1.5 μm as the output waveguide width is 0.4 μm.
 [doi:10.1063/1.3431400]

I. INTRODUCTION

In the past decade, square optical microcavities have attracted great attention[1–12] due to the potential applications in microlasers and high finesse add-drop filters, which are the important components of photonic integrated circuits. The microsquare cavity was discussed for the application of add-drop filters ten years ago.[1] Multimode resonances were observed in square-shaped microcavities in fused silica.[2] Mode selection was investigated in a square-shaped layered microcavity laser.[3] Whispering-gallery mode lasing was observed in a gain-coated square microcavity with round corners.[4] Mode characteristics of square cavities in air were analyzed and simulated,[5] and mode Q factor was calculated by far-field emission based on the analytical near field distribution.[6] The effects of imperfect boundary were studied by the Muller boundary integral equation technique and the finite-difference time-domain (FDTD) technique,[7,8] and mode characteristics were simulated for the square cavities by three dimensional FDTD technique.[9,10] In addition, corner-cut square microcavities were investigated for realizing traveling-wavelike filtering responses.[11–13] Recently, lasing in metallically coated nanolasers was realized,[14] and nanocavity surrounded by a low-refractive-index insulating layer and metal Au was investigated.[15] InGaAsP/InP square microcavity lasers laterally confined by SiO_2 and *p*-electrode were fabricated with an output waveguide connected to the middle of one side of the square.[16] Up to seven distinct transverse modes were observed in the lasing spectrum of a square microlaser with the side length of 20 μm.[17] Numerical results indicated that Au layer can enhance the mode confinement, but the Ti layer used to improve the adherence of the *p*-electrode will result in additional dissipative loss.[18,19]

In this paper, the mode characteristics of square microcavities with an output waveguide, laterally confined by an insulating layer SiO_2 and an Au layer, are numerically simulated by two-dimensional (2D) FDTD technique for Fabry–Pérot type modes and whispering-gallery type modes. The mode Q factors are calculated for the confined modes with different symmetries. The numerical results indicate that the mode Q factors are mainly determined by the mode coupling between the confined modes in the square cavity and guided modes in the output waveguide.

II. FDTD SIMULATION MODEL

The microsquare lasers were fabricated from an edge-emitting laser wafer by dry etching technique with the etched sidewalls surrounded by SiO_2 and the *p*-electrode.[16,17] Under effective index approximation, the lasers can be modeled as a 2D square cavity with the effective index $n_0=3.2$ for the multilayer slab waveguide of the laser wafer. The schematic of the 2D square cavity with an output waveguide connected to the middle of one side is shown in Fig. 1(a), the microcavity is laterally confined by SiO_2 and Au layers with refractive index $n_1=1.45$ and $n_2=0.18+10.2i$ at the wavelength 1.55 μm.[20] Figure 1(b) shows the cross sectional view of the device structure. The thicknesses of the SiO_2 and

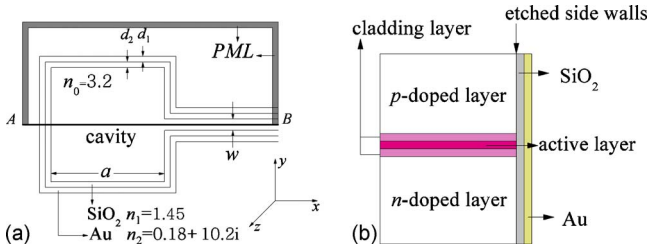

FIG. 1. (Color online) (a) Schematic of a 2D square cavity with an output waveguide connected to the middle of one side, laterally confined by an insulating layer SiO_2 and a Au layer with refractive index $n_1=1.45$ and $n_2=0.18+10.2i$, respectively. (b) The cross sectional view of the device structure.

[a)]Electronic mail: yzhuang@semi.ac.cn.

Au layers are d_1 and d_2, respectively, and the side length of the square cavity and the width of the output waveguide are a and w. The influences of the output waveguide on the mode characteristics are investigated by 2D FDTD technique for transverse magnetic (TM) modes. The FDTD simulation is performed on a half of the square cavity under symmetry and antisymmetry conditions, respectively, for the z-directional electric field E_z relative to the symmetry axis AB.[21,22] The perfectly matched absorbing layers shown as the gray areas in Fig. 1(a) are used as the other boundaries to terminate the FDTD computation.[23] The Courant time step $\Delta t=0.0233$ fs and a uniform mesh with cell size of 10 nm are used in the FDTD simulation. The Drude dispersion model is used to model the performance of the electromagnetic fields in the metal layer[21]

$$\varepsilon(\omega)=\varepsilon_\infty+\frac{\omega_p^2}{2i\omega\nu_c-\omega^2}, \tag{1}$$

where the relative permittivity at infinite frequency ε_∞ is set as 1. The reference value $(0.18+10.2i)^2$ of the permittivity ε at the wavelength 1.55 μm is used to determine the plasma frequency ω_p and the collision frequency ν_c.[20] A Gaussian-modulated cosine impulse

$$p(x_0,y_0,t)=\exp\left[-\frac{(t-t_0)^2}{t_w^2}\right]\cos(2\pi ft) \tag{2}$$

is added to electric component E_z at a point (x_0,y_0) of low symmetry inside the square cavity for simulating TM modes, where t_0 and t_w are the times of center and half-width of the pulse and f is the center frequency. The time variation in $E_z(t)$ is recorded at an arbitrarily selected monitor point inside the square cavity as a FDTD output, then the Padé approximation with Baker's algorithm is used to transform the FDTD output from the time-domain to the frequency-domain,[24] and finally the mode frequency and Q factor are calculated from the peak frequency and the ratio of the peak frequency to the corresponding 3-dB bandwidth by fitting the peak of the intensity spectra with a Lorentzian function.

III. FABRY–PÉROT TYPE MODES

For a square cavity with the side length of 4 μm surrounded by 0.2 μm SiO_2 and 0.2 μm Au, we calculate mode Q factors as the functions of the width of the output waveguide. Confined modes are expressed as TM(p,q) with that p and q are the numbers of wave nodes in the two orthogonal sides of the square cavity. Here, the modes TM(p,q) are roughly marked as Fabry–Pérot type modes if p or q is near zero, and as whispering-gallery type modes if $p\approx q$. The mode Q factors versus the width of the output waveguide w are plotted in Fig. 2 for (a) odd modes TM(p,15) and (b) even modes TM(p,16) with $p=0$ to 5. The odd and even modes have asymmetric and symmetric E_z relative to the axis AB, respectively. TM(p,15) and TM(p,16) are similar to the fundamental, the first,…, and the fifth order transverse modes in the Fabry–Pérot cavity as $p=0,1,\ldots$, and 5. The mode Q factors of the odd modes TM(p,15) keep constants as the width of the output waveguide w is less than 0.2 μm, because they cannot couple with the only guided mode in the output waveguide. The even modes TM(p,16) can couple with the fundamental mode in the output waveguide, so mode Q factors of some even modes decrease greatly even w is less than 0.2 μm. The mode Q factors of the odd modes TM(0,15) to TM(3,15) and TM(5,15) are larger than 6000 as the width w is less than 0.7 μm, and those of the even modes TM(0, 16) to TM(5, 16) are larger than 6000 as the width w is less than 0.4 μm. In Fig. 2(b), the mode Q factors quickly decrease as w is larger than 0.4 μm due to the appearance of the second even guided mode in the output waveguide. The mode frequencies are 176.93 and 189.72 THz for TM(0,15) and TM(5,15), and 188.28 and 200.38 THz for TM(0, 16) and TM(5, 16) as $w=0$. The frequencies of the Fabry–Pérot type modes are little influenced by the output waveguide, such as the frequency of TM(5, 15) varies from 189.72 to 189.59 THz as w increases from 0 to 1.2 μm.

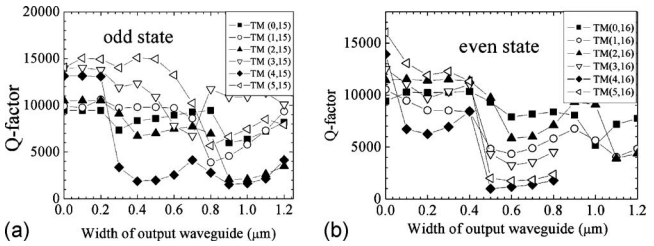

FIG. 2. Mode Q factors vs the width of the output waveguide for Fabry–Pérot type (a) odd modes TM(p,15) and (b) even modes TM(p,16) with $p=0$ to 5.

Choosing a narrow-bandwidth exciting source centered at a resonant mode frequency, we can simulate the mode field distribution for each guided mode by FDTD technique. The obtained distributions of the electric field E_z are plotted in Fig. 3 for (a) TM(0,15) and (b) TM(0,16) in the 4-μm-side square cavity with a 0.9-μm-wide output waveguide. The corresponding mode Q factors are 6.0×10^3 and 8.0×10^3 for TM(0,15) and TM(0,16) as $w=0.9$ μm. For the Fabry–Pérot type modes TM(0,15) and TM(0,16), the output waveguide is located in the weak field region corresponding to the tail of the transverse mode distribution, so the coupling into the output waveguide is very weak and the modes still have high Q factors as $w=0.9$ μm. Their degenerate modes TM(15,0) and TM(16,0), which almost transmit in the x direction, strongly couple into the output waveguide and have very small mode Q factors. The FDTD simulation cannot yield the field patterns for TM(15,0) and TM(16,0) modes in the square resonator with a wide output waveguide. The results

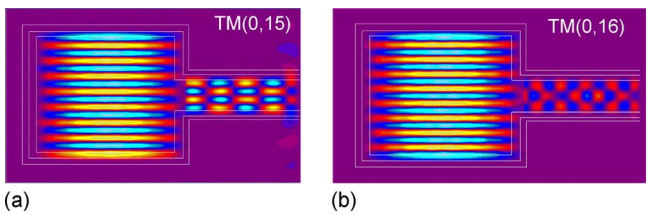

FIG. 3. (Color online) The distributions of electric field E_z for the fundamental modes of (a) TM(0,15) and (b) TM(0,16) as $w=0.9$ μm. Field amplitudes in the output waveguide are magnified five times.

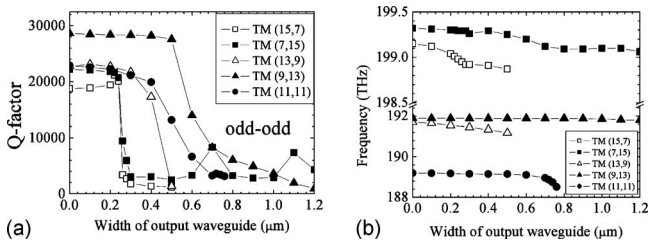

FIG. 4. (a) Mode Q factors and (b) resonant frequencies vs the width of output waveguide for whispering-gallery type modes.

show that the Fabry–Pérot type modes can be used for realizing directional emission as the side walls of the square cavity are surrounded by the SiO_2 and Au layers.

IV. WHISPERING-GALLERY TYPE MODES

The whispering-gallery modes are considered as the confined mode with the incident angles of the mode light rays on the boundaries of the cavity are larger than the critical angle of total internal reflection. But the whispering-gallery modes in Ref. 5 were strictly defined as the high Q modes for the square resonator in air with the transverse mode number $m=|p-q|/2-1$, and the longitudinal mode number $l=p+q+4$ or $p+q+2$ as m is even or odd numbers, respectively.[5] In this section, modes with $p+q=22$ and 23 at the wavelength around 1520 nm are considered for modes with different symmetry.

The mode Q factors and the frequencies versus the width of the output waveguide w are plotted in Figs. 4(a) and 4(b) for TM(15,7), TM(7,15), TM(13,9), TM(9,13), and TM(11,11) modes, with odd mode numbers p and q and $p+q=22$. The modes with odd mode numbers have asymmetric mode field E_z relative to the output waveguide, so the mode Q factors keep constant as w is less than 0.2 μm as in Fig. 2(a). The mode Q factors of the whispering-gallery type modes in Fig. 4(a) are about two times of those of the Fabry–Pérot type modes in Fig. 2(a) as w is less than 0.5 μm. However, the mode Q factors of the whispering-gallery type modes decrease more quickly with the increase in the width w than the Fabry–Pérot type modes, and most of the whispering-gallery type modes have Q factors less than 5000 as $w>0.8$ μm. The results indicate that the Fabry–Pérot type modes will compete with the whispering-gallery type modes in the square cavity surrounded by SiO_2 and Au layers with a wide output waveguide. In fact, the laser spectrum of the square microlaser with the side length 20 μm and the width $w=2$ μm has the evidence of the influence of the Fabry–Pérot type modes.[16] In a perfect square cavity without the output waveguide, the degenerate modes TM(p,q) and TM(q,p), as $p-q$ is an even number, will have the same symmetry and couple to form two combined modes. One of the combined modes has mode field distribution asymmetry relative to the square diagonal mirror planes and have much higher Q factor than the other combined mode for the square cavity in air.[5,25] But for the square cavity surrounded by SiO_2 and Au layers, the two combined modes may have the same magnitude of mode Q factors as the width w is zero, and the output waveguide destroys the symmetry of the square cavity and the formation of the combined modes. So we do not express the modes as the combined modes in this paper, but we have different mode frequencies and Q factors for TM(p,q) and TM(q,p) in Fig. 4 at $w=0$, which are corresponding to the results of the combined modes.

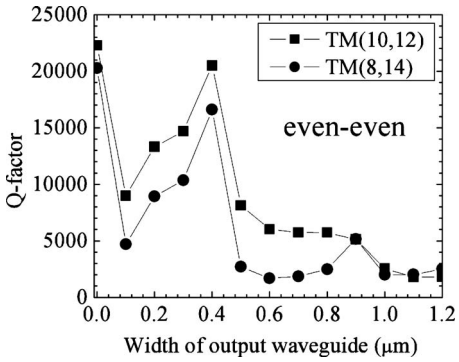

FIG. 5. Mode Q factors vs the width of the output waveguide for TM(10,12) and TM(8,14).

In Fig. 5, we plot the mode Q factors versus the width w for TM(8,14) and TM(10,12) with the mode frequencies of 194.82 and 189.74 THz at $w=0$. The mode Q factors rapidly decrease from 2.0×10^4 and 2.2×10^4 at $w=0$ to 4.7×10^3 and 9.0×10^3 at $w=0.1$ μm for TM(8,14) and TM(10,12), respectively, then increase as w increases from 0.1 to 0.4 μm, and finally quickly decrease as w is larger than 0.4 μm. TM(8,14) and TM(10,12) are the second order and the fundamental transverse modes in the whispering-gallery type mode.[5] So TM(8,14) and TM(10,12) have strong mode field distributions in the middle of the square side, and strong coupling with the fundamental mode of the output waveguide. The distributions of electric field E_z obtained by the FDTD simulation are plotted in Fig. 6 for (a) TM(9,13) and (b) TM(10,12) at $w=0.2$ μm. TM(9,13) has asymmetric field distribution relative to the output waveguide and cannot couple with the fundamental mode in the output waveguide, which is the only guided mode in the output waveguide as $w=0.2$ μm. But TM(10,12) is strongly coupled into the output waveguide, and the corresponding field distribution becomes very weak in the mid points of the four sides of the square cavity. The results indicate that the mode field distribution is greatly influenced by the 0.2-μm-wide output waveguide, i.e., the output waveguide cannot be considered as a perturbation to TM(10,12) mode. The increase in mode Q factor as w increases from 0.1 to 0.4 μm in Fig. 5 can be explained by the modification of mode field pattern, which decreases the mode coupling into the output waveguide.

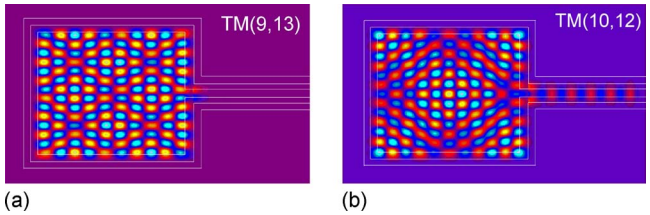

FIG. 6. (Color online) The distributions of electric field E_z for (a) TM(9,13) and (b) TM(10,12) in the square cavity with a 0.2-μm-wide output waveguide. Field amplitudes in the output waveguide are magnified five times.

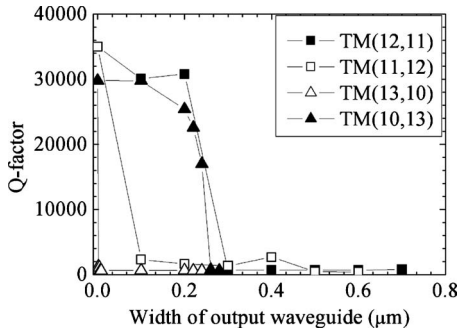

FIG. 7. Mode Q factors vs the width of the output waveguide for TM(11,12) and TM(12,11), TM(10,13), and TM(13,10).

Mode Q factors versus the width w are plotted in Fig. 7 for TM(12,11), TM(11,12), TM(13,10), and TM(10,13) with the mode frequencies of 197.55 and 198.81 THz at $w=0$. These modes have one even and one odd mode numbers, and cannot form the combined modes even in the perfect square cavity. So we have the same mode Q factors in Fig. 7 at $w=0$ for the degenerate modes TM(12,11) and TM(11,12), and TM(13,10) and TM(10,13), respectively. TM(11,12) and TM(13,10) can couple with the even guided modes in the output waveguide, so their mode Q factors decrease quickly as introducing the output waveguide. But TM(12,11) and TM(10,13) can only couple with the odd modes in the output waveguide, and their mode Q factors mainly decrease as w is larger than 0.2 μm corresponding to the appearance of the first order transverse mode in the output waveguide. Furthermore, the mode Q factors in Fig. 7 are almost smaller than 1000 as w is larger than 0.3 μm, much smaller than those in Figs. 4(a) and 5.

Finally, we consider a square cavity with the side length $a=6$ μm. The mode Q factors versus the width w are plotted in Fig. 8 as the circle and square symbols for TM(15,19) and TM(16,18) with the mode frequencies of 193.85 and 192.58 THz at $w=0$. The two modes have mode Q factors larger than 2.0×10^4 as the width w is smaller than 0.4 μm. If the output waveguide can be considered as a perturbation to the mode field pattern, we can expect that the mode Q factor increases with the increase in the side length a by keeping the ratio of w/a as a constant. Because the coupling loss comes from the mode field at the width w, but the stored mode field energy is proportional to the square area a^2. Because a wide output waveguide may greatly influence the mode field pattern as shown in Fig. 6(b), the variation in mode Q factor versus the width w is complicated.

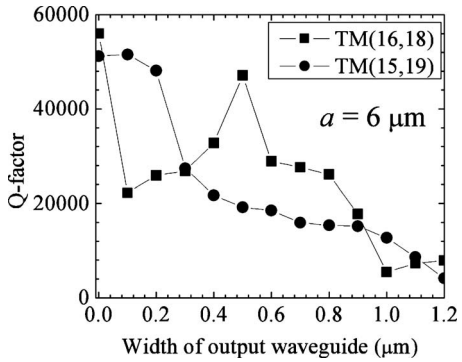

FIG. 8. Mode Q factors vs the width of the output waveguide for TM(15,19) and TM(16,18) in a square cavity with the side length of 6 μm.

V. CONCLUSION

Mode characteristics are investigated by 2D FDTD technique for metallically coated square microcavity with an output waveguide connected to the middle of one side. Fabry–Pérot type modes and whispering-gallery type modes are simulated for the square cavity surrounded by SiO_2 and Au layers. Due to the high reflectivity of the Au layer, the Fabry–Pérot type modes can also have high Q factors in the square cavity, and their Q factors can even larger than those of the whispering-gallery type modes as the width of the output waveguide is larger than 1 μm.

ACKNOWLEDGMENTS

This work was supported by National Nature Science Foundation of China under Grant Nos. 60777028, 60723002, and 60838003, and the Major State Basic Research Program under Grant No. 2006CB302804.

[1] C. Manolatou, M. J. Khan, S. Fan, P. R. Villeneuve, H. A. Haus, and J. D. Joannopoulos, IEEE J. Quantum Electron. **35**, 1322 (1999).
[2] A. W. Poon, F. Courvoisier, and R. K. Chang, Opt. Lett. **26**, 632 (2001).
[3] H. J. Moon, K. An, and J. H. Lee, Appl. Phys. Lett. **82**, 2963 (2003).
[4] H. J. Moon, S. P. Sun, G. W. Park, J. H. Lee, and K. An, Jpn. J. Appl. Phys., Part 2 **42**, L652 (2003).
[5] W. H. Guo, Y. Z. Huang, Q. Y. Lu, and L. J. Yu, IEEE J. Quantum Electron. **39**, 1563 (2003).
[6] W. H. Guo, Y. Z. Huang, Q. Y. Lu, and L. J. Yu, IEEE Photonics Technol. Lett. **16**, 479 (2004).
[7] S. V. Boriskina, T. M. Benson, P. Sewell, and A. I. Nosich, IEEE J. Quantum Electron. **41**, 857 (2005).
[8] Q. Chen, Y. Z. Huang, and L. J. Yu, IEEE J. Quantum Electron. **42**, 59 (2006).
[9] Q. Chen and Y. Z. Huang, J. Opt. Soc. Am. B **23**, 1287 (2006).
[10] Y. D. Yang, Y. Z. Huang, and Q. Chen, IEEE Photonics Technol. Lett. **19**, 1831 (2007).
[11] C. Y. Fong and A. W. Poon, Opt. Express **12**, 4864 (2004).
[12] E. Marchena, S. Y. Shi, and D. Prather, Opt. Express **16**, 16516 (2008).
[13] Q. Chen, Y. D. Yang, and Y. Z. Huang, Opt. Lett. **32**, 967 (2007).
[14] M. T. Hill, Y.-S. Oei, B. Smalbrugge, Y. Zhu, T. de Vries, P. J. van Veldhoven, F. W. M. van Otten, T. J. Eijkemans, J. P. Turkiewicz, H. de Waardt, E. J. Geluk, S.-H. Kwon, Y.-H. Lee, R. Nötzel, and M. K. Smit, Nat. Photonics **1**, 589 (2007).
[15] A. Mizrahi, V. Lomakin, B. A. Slutsky, M. P. Nezhad, L. Feng, and Y. Fainman, Opt. Lett. **33**, 1261 (2008).
[16] Y. Z. Huang, K. J. Che, Y. D. Yang, S. J. Wang, Y. Du, and Z. C. Fan, Opt. Lett. **33**, 2170 (2008).
[17] K. J. Che, Y. D. Yang, and Y. Z. Huang, Appl. Phys. Lett. **96**, 051104 (2010).
[18] Y. D. Yang, Y. Z. Huang, and S. J. Wang, IEEE J. Quantum Electron. **45**, 1529 (2009).
[19] K. J. Che, Y. D. Yang, and Y. Z. Huang, IEEE J. Quantum Electron. **46**, 414 (2010).
[20] M. A. Ordal, L. L. Long, R. J. Bell, S. E. Bell, R. R. Bell, R. W. Alexander, Jr., and C. A. Ward, Appl. Opt. **22**, 1099 (1983).
[21] A. Taflove and S. C. Hagness, *Computational Electrodynamics: The Finite-Difference Time-Domain Method*, 3rd ed. (Artech House, Norwood, MA, 2005).
[22] S. C. Hagness, D. Rafizadeh, S. T. Ho, and A. Taflove, J. Lightwave Technol. **15**, 2154 (1997).
[23] J. P. Berenger, J. Comput. Phys. **114**, 185 (1994).
[24] W. H. Guo, W. J. Li, and Y. Z. Huang, IEEE Microw. Wirel. Compon. Lett. **11**, 223 (2001).
[25] Y. D. Yang and Y. Z. Huang, IEEE J. Quantum Electron. **43**, 497 (2007).